Electric Power Components and Systems, 32:75–91, 2004

ISSN: 1532-5008 print/1532-5016 online
DOI: 10.1080/15325000490196915

Taylor & Francis
Taylor & Francis Group

Analysis of Power System Stability Enhancement via Excitation and Facts-Based Stabilizers

M. A. ABIDO
Y. L. ABDEL-MAGID

Electrical Engineering Department
King Fahd University of Petroleum and Minerals
Dhahran, Saudi Arabia

Power system stability enhancement via excitation and FACTS-based stabilizers is thoroughly investigated in this paper. This study presents a singular value decomposition–based approach to assess and measure the controllability of the poorly damped electromechanical modes by different control inputs. The design problem of a power system stabilizer and different FACTS-based stabilizers is formulated as an optimization problem. An eigenvalue-based objective function to increase the system damping and improve the system response is developed. Then, a real-coded genetic algorithm is employed to search for optimal controller parameters. In addition, the damping characteristics of the proposed schemes are also evaluated in terms of the damping torque coefficient with different loading conditions for better understanding of the coordination problem requirements. The proposed stabilizers are tested on a weakly connected power system with different loading conditions. The damping torque coefficient analysis, nonlinear simulation results, and eigenvalue analysis show the effectiveness and robustness of the proposed control schemes over a wide range of loading conditions.

Keywords power system stability, FACTS devices, genetic algorithms

1. Introduction

Since the 1960s low-frequency oscillations have been observed when large power systems are interconnected by relatively weak tie lines. These oscillations may sustain and grow to cause system separation if no adequate damping is available [1, 2].

Although power system stabilizers (PSSs) provide supplementary feedback stabilizing signals, they suffer a drawback of being liable to cause great variations in the voltage profile, and they may even result in leading power factor operation under severe disturbances. Recent advances in power electronics have led to the development of flexible alternating current transmission systems (FACTS). Generally, a potential motivation for the accelerated use of FACTS devices is the deregulation

Manuscript received in final form on 6 May 2002.
The authors acknowledge the support of King Fahd University of Petroleum & Minerals via funded Project # FT/2000-25.
Address correspondence to M. A. Abido, Electrical Engineering Department, King Fahd University of Petroleum and Minerals, KFUPM Box 183, Dhahran 31261, Saudi Arabia. E-mail: mabido@kfupm.edu.sa

environment in contemporary utility business. Along with primary function of the FACTS devices, the real power flow can be regulated to mitigate the low-frequency oscillations and enhance power system stability. This suggests that FACTS will find new applications as electric utilities merge and as the sale of bulk power between distant and ill-interconnected partners become more widespread.

Recently, several FACTS devices have been implemented and installed in practical power systems such as the static VAR compensator (SVC) [3–4], thyristor-controlled series capacitor (TCSC) [5–6], and thyristor-controlled phase shifter (TCPS) [7–8]. In the literature a little work has been done on the coordination problem investigation of excitation and FACTS-based stabilizers. Mahran et al. [9] presented a coordinated PSS and SVC control for a synchronous generator. However, the proposed approach uses recursive least squares identification, which reduces its effectiveness for online applications. Rahim and Nassimi [10] presented optimum feedback strategies for both SVC and exciter controls. However, the proposed controller requires some or all states to be measurable or estimated. Moreover, it leads to a centralized controller for multimachine power systems, which reduces its applicability and reliability. Noorozian and Anderson [11] presented a comprehensive analysis of damping of power system electromechanical oscillations using TCSC, TCPS, and SVC, where the impact of transmission line loading and load characteristics on the damping effect of these devices have been discussed. Hiyama et al. [12] presented a coordinated fuzzy logic–based scheme for PSS and switched series capacitor modules to enhance overall power system stability. The results were promising in the sense that the power system stability region can be greatly extended. Wang and Swift [13] have discussed the damping torque contributed by SVC, TCSC, and TCPS where several important points have been analyzed and confirmed through simulations. However, all controllers were assumed proportional, and no efforts have been done toward the controller design. On the other hand, it is necessary to measure the electromechanical mode controllability to assess the effectiveness of different controllers and form a clear idea about the coordination problem requirements.

In this study excitation and FACTS-based stabilizers are considered to enhance the damping of low-frequency modes. A controllability measure based on singular value decomposition (SVD) is introduced in this work to identify the most effective stabilizer. The stabilizer design problem is transformed into an optimization problem where the real-coded genetic algorithm (RCGA) will be applied to search for the optimal parameter settings. The effectiveness of the proposed stabilizers in enhancing the power system transient stability over a wide range of loading condition is examined. In addition, the damping torque coefficient is evaluated with the proposed stabilizers for better understanding of coordination problem requirements. For completeness, the eigenvalue analysis and nonlinear simulation results are carried out to demonstrate the effectiveness of the proposed stabilizers to enhance system damping.

2. Power System Model

2.1. Generator

In this study a single machine infinite bus system as shown in Figure 1 is considered. The generator is equipped with a PSS, and the system has TCSC, TCPS, and SVC

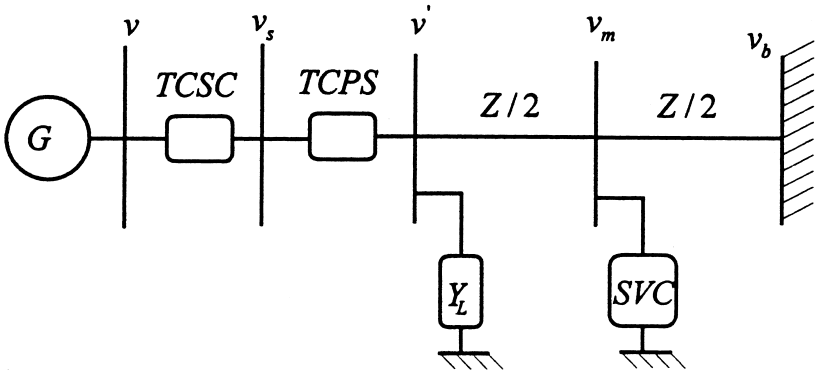

Figure 1. Single machine infinite bus system.

as shown in Figure 1. The line impedance is $Z = R + jX$, and the generator has a local load of admittance $Y_L = g + jb$. The generator is represented by the third-order model comprising of the electromechanical swing equation and the generator internal voltage equation [1, 2]. The swing equation is divided into the following equations:

$$\rho\delta = \omega_b(\omega - 1), \tag{1}$$

$$\rho\omega = \frac{P_m - P_e - D(\omega - 1)}{M}, \tag{2}$$

where, P_m and P_e are the input and output powers of the generator, respectively; M and D are the inertia constant and damping coefficient, respectively; δ and ω are the rotor angle and speed, respectively; and ρ is the derivative operator d/dt. The output power of the generator can be expressed in terms of the d-axis and q-axis components of the armature current, i, and terminal voltage, v, as

$$P_e = v_d i_d + v_q i_q. \tag{3}$$

The internal voltage, E'_q, equation is

$$\rho E'_q = \frac{E_{fd} - (x_d - x'_d)i_d - E'_q}{T'_{do}}. \tag{4}$$

Here E_{fd} is the field voltage; T'_{do} is the open circuit field time constant; and x_d and x'_d are d-axis reactance and d-axis transient reactance of the generator, respectively.

2.2. Exciter and PSS

The IEEE type-ST1 excitation system shown in Figure 2 is considered. It can be described as

$$\rho E_{fd} = \frac{K_A(V_{ref} - v + u_{PSS}) - E_{fd}}{T_A} \tag{5}$$

where, K_A and T_A are the gain and time constant of the excitation system, respectively; and V_{ref} is the reference voltage. As shown in Figure 2, a conventional

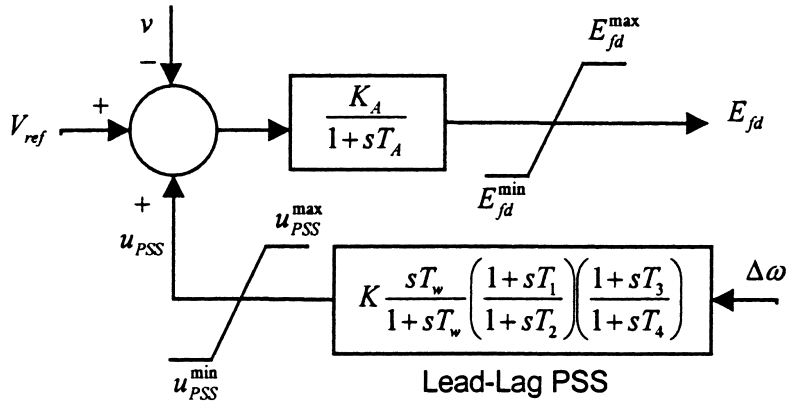

Figure 2. IEEE type-ST1 excitation system with PSS.

lead-lag PSS is installed in the feedback loop to generate a stabilizing signal u_{PSS}. In equation (5), the terminal voltage v can be expressed as

$$v = (v_d^2 + v_q^2)^{1/2}, \tag{6}$$

$$v_d = x_q i_q, \tag{7}$$

$$v_q = E'_q - x'_d i_d, \tag{8}$$

where x_q is the q-axis reactance of the generator.

2.3. FACTS-Based Stabilizers

Figure 3 illustrates the block diagram of an SVC with a lead-lag compensator. The susceptance of the SVC, B_{SVC}, can be expressed as

$$\rho B_{SVC} = \frac{K_s(B_{ref} - u_{SVC}) - B_{SVC}}{T_S}, \tag{9}$$

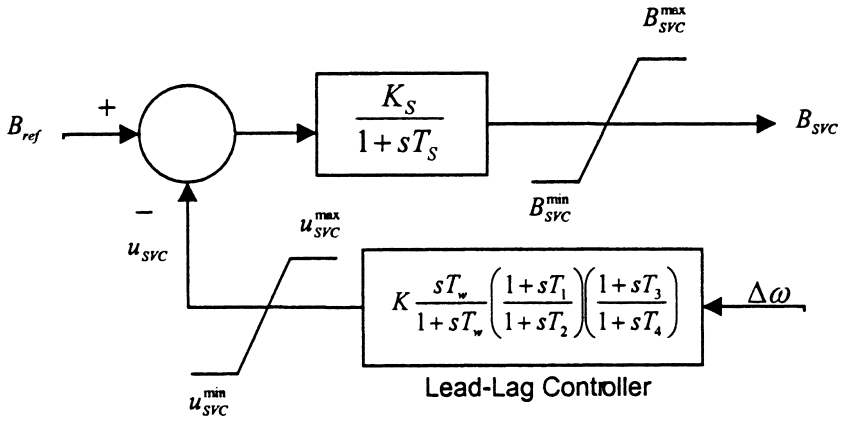

Figure 3. SVC with lead-lag controller.

where B_{ref} is the reference susceptance of SVC; and K_s and T_s are the gain and time constant of the SVC. As shown in Figure 3, a conventional lead-lag controller is installed in the feedback loop to generate the SVC stabilizing signal u_{SVC}. The same controller structure used in Figure 3 is applied for TCSC and TCPS by replacing SVC susceptance B_{SVC} by TCSC reactance X_{TCSC} and TCPS angle Φ_{TCPS}, respectively. Similar expressions for X_{TCSC} and Φ_{TCPS} can be expressed as follows

$$\rho X_{TCSC} = \frac{K_s(X_{ref} - u_{TCSC}) - X_{TCSC}}{T_s}, \tag{10}$$

$$\rho \Phi_{TCPS} = \frac{K_s(\Phi_{ref} - u_{TCPS}) - \Phi_{TCPS}}{T_s}. \tag{11}$$

2.4. Linearized Model

In the design of electromechanical mode damping controllers, the linearized incremental model around a nominal operating point is usually employed [1–2]. Linearizing the expressions of i_d and i_q and substituting into the linear form of equations (1)–(11) yield the following linearized power system model:

$$\begin{bmatrix} \rho\Delta\delta \\ \rho\Delta\omega \\ \rho\Delta E'_q \\ \rho\Delta E_{fd} \end{bmatrix} = \begin{bmatrix} 0 & 377 & 0 & 0 \\ -\frac{K_1}{M} & -\frac{D}{M} & -\frac{K_2}{M} & 0 \\ -\frac{K_4}{T'_{do}} & 0 & -\frac{K_3}{T'_{do}} & \frac{1}{T'_{do}} \\ -\frac{K_A K_5}{T_A} & 0 & -\frac{K_A K_6}{T_A} & -\frac{1}{T_A} \end{bmatrix} \begin{bmatrix} \Delta\delta \\ \Delta\omega \\ \Delta E'_q \\ \Delta E_{fd} \end{bmatrix}$$
$$+ \begin{bmatrix} 0 & 0 & 0 & 0 \\ 0 & -\frac{K_{pB}}{M} & \frac{K_{pX}}{M} & -\frac{K_{p\Phi}}{M} \\ 0 & -\frac{K_{qB}}{T'_{do}} & -\frac{K_{qX}}{T'_{do}} & -\frac{K_{q\Phi}}{T'_{do}} \\ \frac{K_A}{T_A} & -\frac{K_A K_{vB}}{T_A} & -\frac{K_A K_{vX}}{T_A} & -\frac{K_A K_{v\Phi}}{T_A} \end{bmatrix} \begin{bmatrix} u_{PSS} \\ \Delta B_{SVC} \\ \Delta X_{TCSC} \\ \Delta \Phi_{TCPS} \end{bmatrix}. \tag{12}$$

In short,

$$\rho X = AX + HU. \tag{13}$$

Here, the state vector X is $[\Delta\delta, \Delta\omega, \Delta E'_q, \Delta E_{fd}]^T$, and the control vector U is $[u_{PSS}, \Delta B_{SVC}, \Delta X_{TCSC}, \Delta\Phi_{TCPS}]^T$. The block diagram of the linearized power system model is depicted as shown in Figure 4 where K_1–K_6, K_p, K_q, and K_v are

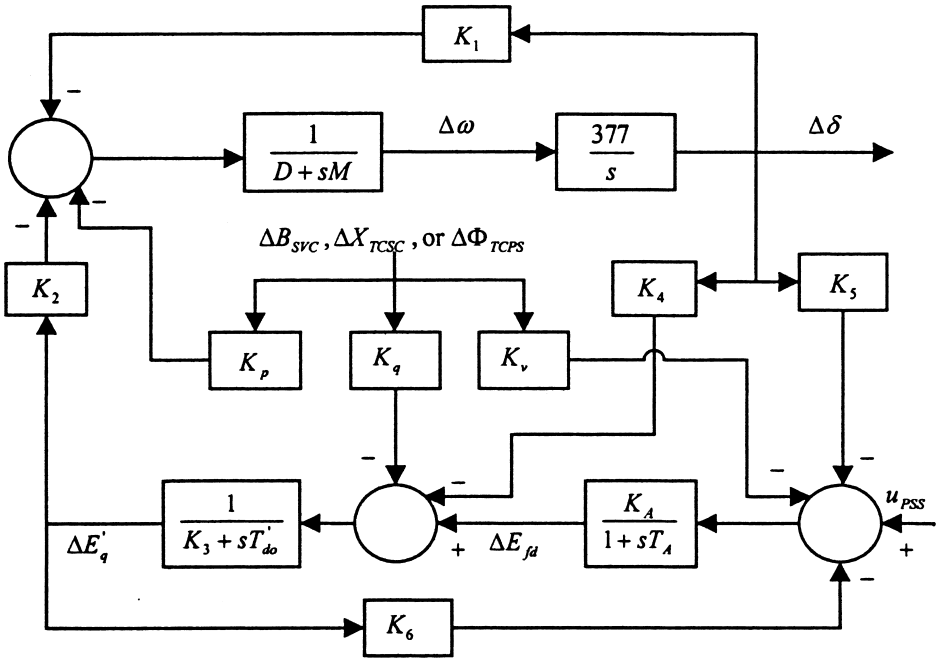

Figure 4. Block diagram of the linearized model.

linearization constants defined as

$$K_1 = \frac{\partial P_e}{\partial \delta}, \qquad K_2 = \frac{\partial P_e}{\partial E'_q}, \qquad K_p = \frac{\partial P_e}{\partial F},$$
$$K_4 = \frac{\partial E_q}{\partial \delta}, \qquad K_3 = \frac{\partial E_q}{\partial E'_q}, \qquad K_q = \frac{\partial E_q}{\partial F}, \tag{14}$$
$$K_5 = \frac{\partial v}{\partial \delta}, \qquad K_6 = \frac{\partial v}{\partial E'_q}, \qquad K_v = \frac{\partial v}{\partial F},$$

where F is B_{SVC}, X_{TCSC}, or Φ_{TCPS}.

3. The Proposed Approach

3.1. Electromechanical Mode Identification

The state equations of the linearized model given in equation (13) can be used to determine the eigenvalues of the system matrix A. Out of these eigenvalues, there is a mode of oscillations related to machine inertia. For the stabilizers to be effective, it is extremely important to identify the eigenvalue associated with the electromechanical mode. In this study the participation factors method [14] is used.

3.2. Controllability Measure

To measure the controllability of the electromechanical mode by a given input, the singular value decomposition (SVD) is employed in this study. Mathematically, if

G is an $m \times n$ complex matrix, then there exist unitary matrices W and V with dimensions of $m \times m$ and $n \times n$ respectively such that G can be written as

$$G = W \sum V^H, \tag{15}$$

where

$$\sum = \begin{bmatrix} \sum\limits_1 & 0 \\ 0 & 0 \end{bmatrix}, \quad \begin{array}{l} \sum\limits_1 = diag(\sigma_1, \ldots, \sigma_r) \\ \text{with } \sigma_1 \geq \cdots \geq \sigma_r \geq 0 \end{array}, \tag{16}$$

where $r = \min\{m, n\}$ and $\sigma_1, \ldots, \sigma_r$ are the singular values of G.

The minimum singular value σ_r represents the distance of the matrix G from the all matrices with a rank of $r-1$. This property can be utilized to quantify modal controllability [15]. In this study the matrix H in equation (13) can be written as $H = [h_1, h_2, h_3, h_4]$, where h_i is the column of matrix H corresponding to the ith input. The minimum singular value of the matrix $[\lambda I - Ah_i]$ indicates the capability of the ith input to control the mode associated with the eigenvalue λ. As a matter of fact, the higher the minimum singular value, the higher the controllability of this mode by the input considered. Having been identified, the controllability of the electromechanical mode can be examined with all inputs to identify the most effective one to control that mode.

3.3. Stabilizer Design

A widely used conventional lead-lag structure for both excitation and FACTS-based stabilizers, shown in Figures 2 and 3, is considered. In this structure the washout time constant T_w and the time constants T_2 and T_4 are usually prespecified. The controller gain K and time constants T_1 and T_3 are to be determined. In this study the input signal of all proposed controllers is the speed deviation $\Delta\omega$.

In the stabilizer design process, it is aimed to maximize the damping ratio of the poorly damped electromechanical mode eigenvalues. Therefore, the following eigenvalue-based objective function J is used:

$$J = \min\{\zeta : \zeta \in \zeta\text{s of electromechanical modes}\}, \tag{17}$$

where ζ is the damping ratio of the electromechanical mode eigenvalue. In the optimization process, it is aimed to *Maximize* J while satisfying the problem constraints that are the optimized parameter bounds. Therefore, the design problem can be formulated as the following optimization problem.

$$\begin{aligned} &\textit{Maximize } J \\ &\textit{Subject to} \qquad (18) \\ &K^{\min} \leq K \leq K^{\max}, \qquad (19) \\ &T_1^{\min} \leq T_1 \leq T_1^{\max}, \qquad (20) \\ &T_3^{\min} \leq T_3 \leq T_3^{\max}. \qquad (21) \end{aligned}$$

The proposed approach employs RCGA to solve this optimization problem and search for an optimal or near optimal set of the optimized parameters.

3.4. Damping Torque Coefficient Calculation

To assess the effectiveness of the proposed stabilizers, the damping torque coefficient is evaluated and analyzed. The torque can be decomposed into synchronizing and damping components as follows:

$$\Delta T_e(t) = K_{syn}\Delta\delta(t) + K_d\Delta\omega(t), \tag{22}$$

where K_{syn} and K_d are the synchronizing and damping torque coefficients, respectively. It is worth mentioning that K_d is a damping measure to the electromechanical mode of oscillations [16].

To calculate K_{syn} and K_d, the error between the actual torque deviation and that obtained by summing both components can be defined as

$$E(t) = \Delta T_e(t) - (K_{syn}\Delta\delta(t) + K_d\Delta\omega(t)). \tag{23}$$

Then K_{syn} and K_d are computed to minimize the sum of the squared errors over the simulation period t_{sim} as

$$\sum^{N}[E]^2 = \sum^{N}[\Delta T_e - (K_{syn}\Delta\delta + K_d\Delta\omega)]^2, \tag{24}$$

where $t_{sim} = N \times T_{samp}$, T_{samp} is the sampling period. Thus, these coefficients should satisfy

$$\frac{\partial}{\partial K_{syn}}\sum^{N}[E]^2 = 0 \qquad \text{and} \qquad \frac{\partial}{\partial K_d}\sum^{N}[E]^2 = 0, \tag{25}$$

which yields

$$\sum^{N}\Delta T_e\Delta\delta = K_{syn}\sum^{N}[\Delta\delta]^2 + K_d\sum^{N}[\Delta\omega.\Delta\delta], \tag{26}$$

$$\sum^{N}\Delta T_e\Delta\omega = K_d\sum^{N}[\Delta\omega]^2 + K_{syn}\sum^{N}[\Delta\omega.\Delta\delta]. \tag{27}$$

Solving equations (26) and (27), K_{syn} and K_d can be calculated.

4. Implementation

4.1. Real-Coded Genetic Algorithm

Due to difficulties of binary representation when dealing with continuous search space with a large dimension, the proposed approach has been implemented using a real-coded genetic algorithm (RCGA) [17]. A decision variable x_i is represented by a real number within its lower limit a_i and upper limit b_i: $x_i \in [a_i, b_i]$. The RCGA crossover and mutation operators are described as follows.

Crossover: A blend crossover operator (BLX-α) has been employed in this study. This operator starts by choosing randomly a number from the interval $[x_i - \alpha(y_i - x_i), y_i + \alpha(y_i - x_i)]$, where x_i and y_i are the ith parameter values of the parent solutions and $x_i < y_i$. To ensure the balance between exploitation and exploration of the search space, $\alpha = 0.5$ is selected. This operator is depicted in Figure 5.

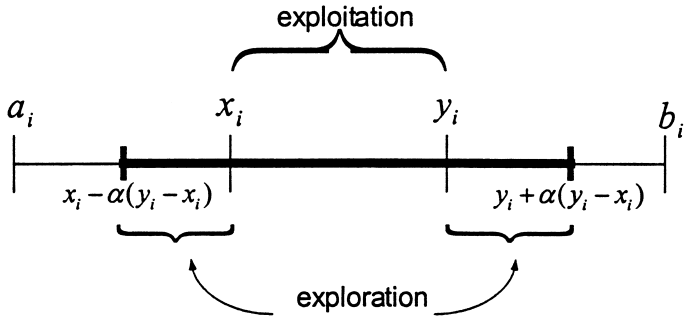

Figure 5. Blend crossover operator (BLX-α).

Mutation: The nonuniform mutation operator has been employed in this study. In this operator the new value x_i' of the parameter x_i after mutation at generation t is given as

$$x_i' = \begin{cases} x_i + \Delta(t, b_i - x_i) & \text{if } \tau = 0 \\ x_i - \Delta(t, x_i - a_i) & \text{if } \tau = 1 \end{cases}, \tag{28}$$

$$\Delta(t, y) = y(1 - r^{\left(1 - \frac{t}{g_{\max}}\right)^{\beta}}), \tag{29}$$

where τ is a binary random number, r is a random number $r \in [0, 1]$, $g_{\max}$ is the maximum number of generations, and β is a positive constant chosen arbitrarily. In this study $\beta = 5$ was selected. This operator gives a value $x_i' \in [a_i, b_i]$ such that the probability of returning a value close to x_i increases as the algorithm advances. This makes uniform search in the initial stages where t is small and very locally at the later stages.

4.2. RCGA Application

RCGA has been applied to search for optimal settings of the optimized parameters of the proposed control schemes. In our implementation the crossover and mutation probabilities of 0.9 and 0.01, respectively, are found to be quite satisfactory. The number of individuals in each generation is selected to be 100. In addition, the search will terminate if the best solution does not change for more than 50 generations or the number of generations reaches 500. The computational flow chart of the proposed design approach is shown in Figure 6.

5. Results and Discussions

5.1. Settings of the Proposed Stabilizers

The proposed approach has been implemented on a weakly connected power system. The detailed data of the power system used in this study is given in the Appendix. The convergence rate of the objective function J with the number of generations is shown in Figure 7 for all proposed stabilizers. The stabilizer parameters have been optimized to improve the damping ratio of the electromechanical mode eigenvalue.

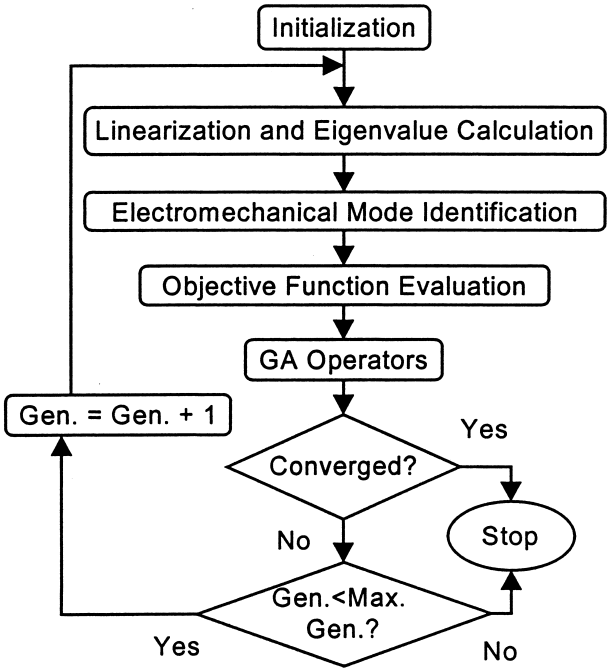

Figure 6. Flow chart of the proposed design approach.

The final settings of the optimized parameters for the proposed stabilizers are given in Table 1. The system eigenvalues without and with the proposed stabilizers are given in Table 2, where the first row represents the electromechanical mode eigenvalues. It is clear that the electromechanical mode is unstable without control while the system stability is greatly enhanced with the proposed stabilizers.

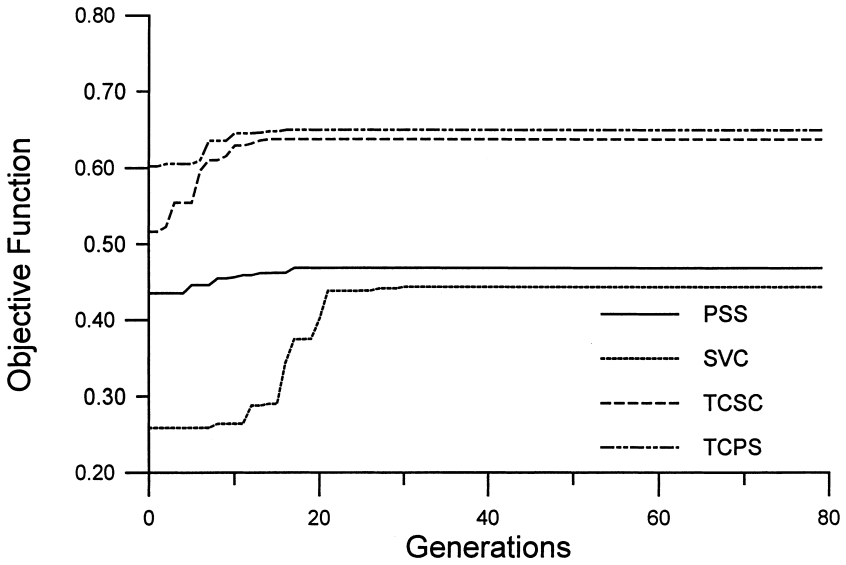

Figure 7. Objective function convergence.

Table 1
Optimal parameter settings of the proposed stabilizers

	PSS	*SVC*	*TCSC*	*TCPS*
K	17.896	98.647	99.848	99.760
T_1	0.2770	0.9587	0.0596	0.0720
T_2	0.1000	0.3000	0.1000	0.1000
T_3	—	0.0114	—	—
T_4	—	0.3000	—	—

5.2. Electromechanical Mode Controllability Measure

With each input signal given in equation (13), the minimum singular value $\sigma_{\min}$ has been estimated to measure the controllability of the electromechanical mode from that input. Figure 8 shows $\sigma_{\min}$ with loading conditions over the range of $P_e = [0.05 - 1.4]$ pu and $Q \in \{-0.4, 0.4\}$ pu. It can be seen that

1. The mode controllability is almost the same in case of PSS and SVC.
2. The mode is more controllable with TCSC and TCPS compared to PSS and SVC.
3. The mode controllability by TCSC changes almost linearly with the system loading.
4. The mode is most controllable by TCPS and TCSC at light loading and heavy loading, respectively.
5. As Q increases, the mode controllability via TCSC becomes dominant at lower loading levels.

5.3. Damping Torque Coefficient

To evaluate the effectiveness of the proposed stabilizers, the damping torque coefficient has been estimated with each stabilizer. Figure 9 shows K_d versus the loading variations. It can be concluded that

1. The damping of the TCPS is almost independent of loading variations.
2. The damping of the TCSC increases linearly with P_e.
3. The SVC provides negative damping at low loading conditions. This becomes more evident with positive Q as shown in Figure 9(c). This confirms the finding presented in [13].

Table 2
System eigenvalues without and with the proposed stabilizers

No control	*PSS*	*SVC*	*TCSC*	*TCPS*
$\mathbf{+0.30 \pm j4.96}$	$-2.71 \pm j5.06^*$	$-2.33 \pm j4.69^*$	$-3.28 \pm j3.96^*$	$-3.05 \pm j3.56^*$
$-10.39 \pm j3.29$	$-3.23 \pm j6.09$	$-2.47 \pm j4.98$	$-6.04 \pm j7.28$	$-7.08 \pm j8.28$
—	-18.31	-20.43	-19.20	-18.03
—	-0.204	-14.21	-12.36	-11.89
—	—	-2.64	-0.21	-0.21
—	—	-0.20	—	—

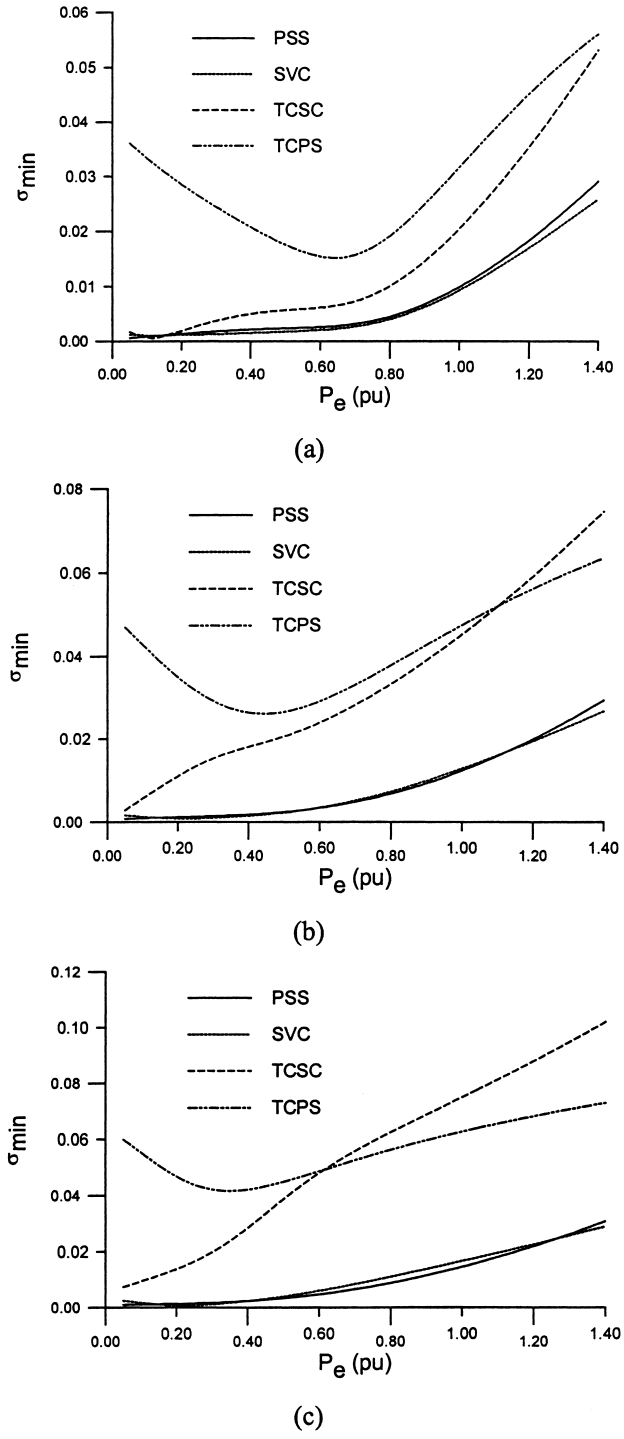

Figure 8. Minimum singular value with loading variations: (a) $Q = -0.4$ pu, (b) $Q = 0.0$ pu, (c) $Q = 0.4$ pu.

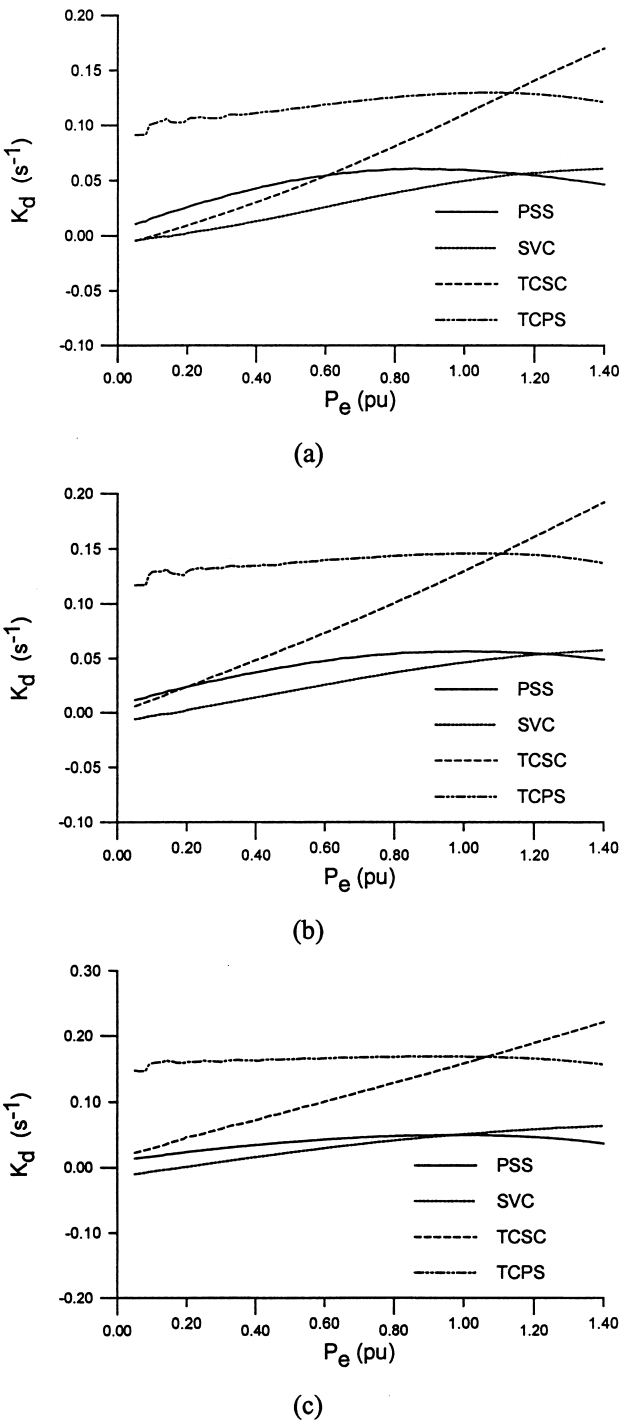

Figure 9. Damping coefficient with the loading variations: (a) $Q = -0.4$ pu, (b) $Q = 0.0$ pu, (c) $Q = 0.4$ pu.

4. It is also observed that TCSC provides negative damping at very low loading levels with leading power factor as shown in Figure 9(a).
5. PSS outperforms the SVC at low loading levels. It also outperforms the TCSC at low loading levels with leading power factor.

5.4. Nonlinear Simulation Results

For completeness and verification, all the proposed stabilizers were tested under different disturbances and loading conditions. Figure 10 shows the system response

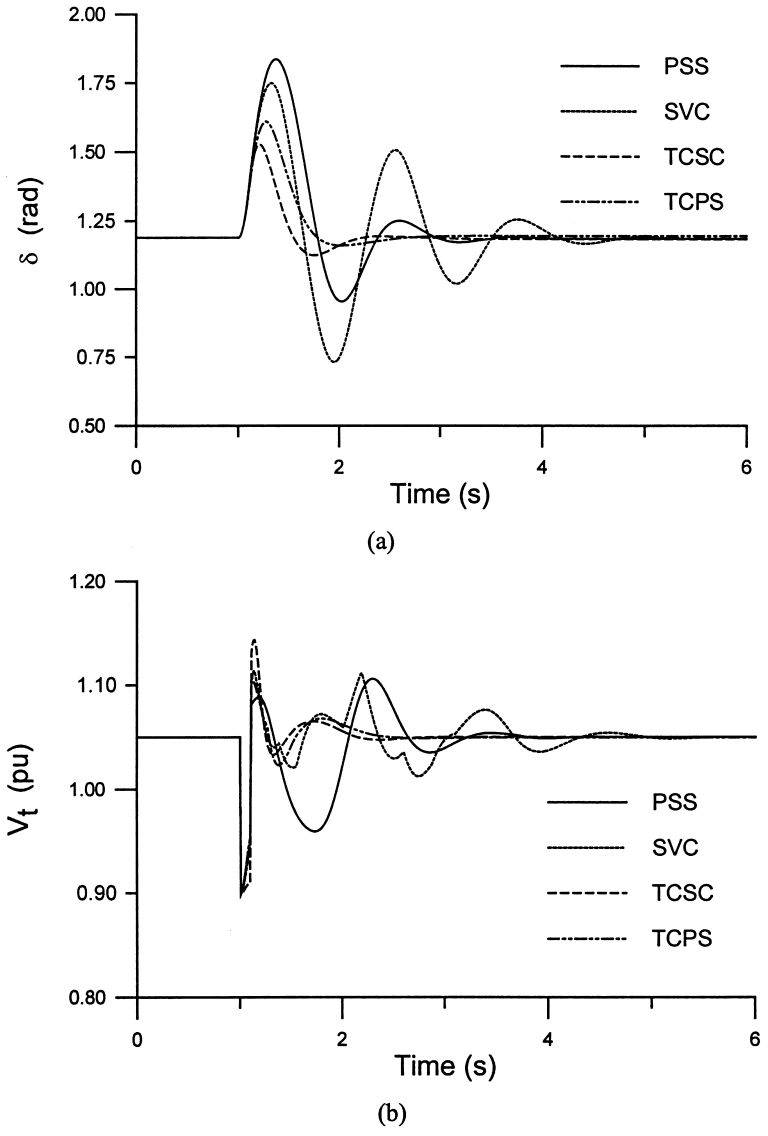

Figure 10. System response for six-cycle fault with nominal loading ($P = 1.0$ pu, $Q = 0.015$ pu): (a) rotor angle response, (b) terminal voltage response.

with six-cycle fault disturbance at the nominal loading condition. It can be seen that the TCPS and TCSC provide the best damping characteristics and enhance greatly the first swing stability. This is found to be consistent with the damping torque coefficient results shown in Figure 9(b). On the other hand, the terminal voltage has great variations with the PSS. The results with a three-cycle fault disturbance at a heavy loading condition are shown in Figure 11. It is clear that the TCSC provides the greatest damping characteristics at this loading. This confirms the findings of Figure 9(c).

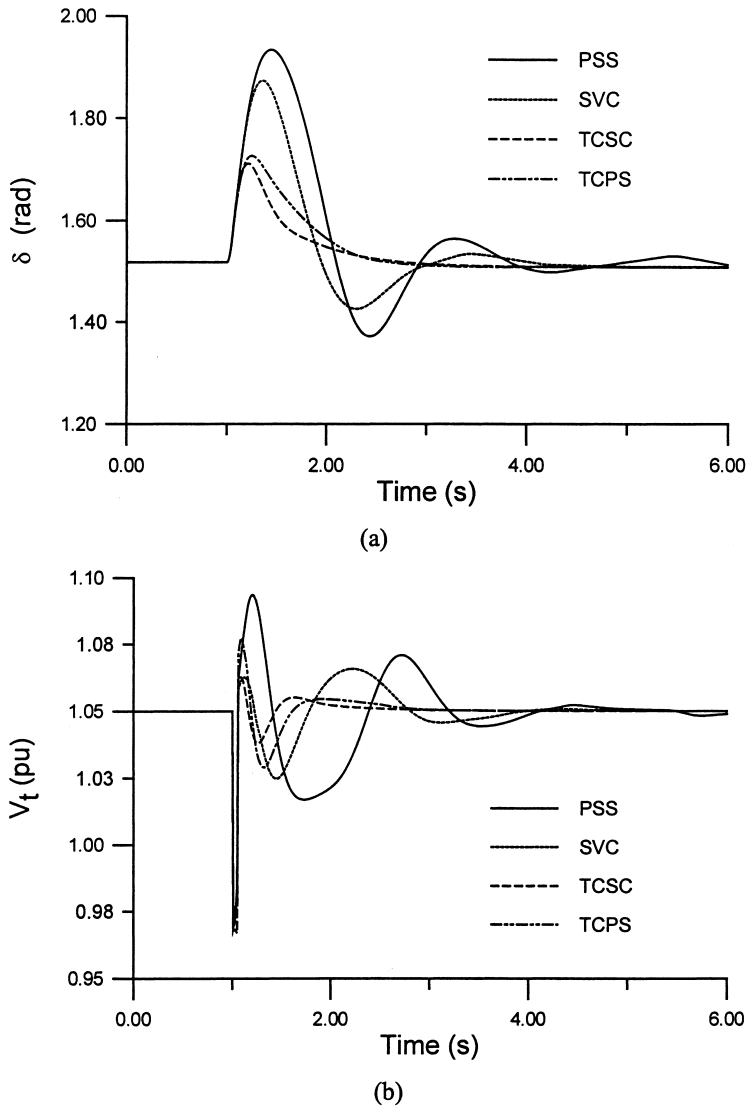

Figure 11. System response for three-cycle fault with heavy loading ($P = 1.1$ pu, $Q = 0.4$ pu): (a) rotor angle response, (b) terminal voltage response.

6. Conclusion

In this study the power system stability enhancement via PSS and FACTS-based stabilizers is presented and discussed. For the proposed stabilizer design problem, an eigenvalue-based objective function to increase the system damping was developed. Then the real-coded genetic algorithm was implemented to search for the optimal stabilizer parameters. In addition, a controllability measure for the poorly damped electromechanical modes using a singular value decomposition approach is proposed to assess the effectiveness of the proposed stabilizers. The damping characteristics of the proposed schemes were also evaluated in terms of the damping torque coefficient. The proposed stabilizers have been tested on a weakly connected power system with different loading conditions. The eigenvalue analysis and nonlinear simulation results show the effectiveness and robustness of the proposed stabilizers to enhance the system stability.

References

[1] Y. N. Yu, *Electric Power System Dynamics*, New York: Academic Press, 1983.
[2] P. W. Sauer and M. A. Pai, *Power System Dynamics and Stability*, Englewood Cliffs, NJ: Prentice Hall, 1998.
[3] A. E. Hammad, "Analysis of power system stability enhancement by static VAR compensators," *IEEE Trans. PWRS*, vol. 1, no. 4, pp. 222–227, 1986.
[4] K. R. Padiyar and R. K. Varma, "Damping torque analysis of static VAR system oscillations," *IEEE Trans. PWRS*, vol. 6, no. 2, pp. 458–465, 1991.
[5] Chen, N. Pahalawaththa, U. Annakkage, and C. Kumble, "Controlled series compensation for improving the stability of multimachine power systems," *IEE Proc.*, pt. C, vol. 142, pp. 361–366, 1995.
[6] J. Chang and J. Chow, "Time optimal series capacitor control for damping inter-area modes in interconnected power systems," *IEEE Trans. PWRS*, vol. 12, no. 1, pp. 215–221, 1997.
[7] A. Edris, "Enhancement of first-swing stability using a high-speed phase shifter," *IEEE Trans. PWRS*, vol. 6, no. 3, pp. 1113–1118, 1991.
[8] F. Jiang, S. S. Choi, and G. Shrestha, "Power system stability enhancement using static phase shifter," *IEEE Trans. PWRS*, vol. 12, pp. 207–214, 1997.
[9] A. R. Mahran, B. W. Hogg, and M. L. El-Sayed, "Coordinated control of synchronous generator excitation and static VAR compensator," *IEEE Trans. Energy Conversion*, vol. 7, pp. 615–622, 1992.
[10] A. Rahim and S. Nassimi, "Synchronous generator damping enhancement through coordinated control of exciter and SVC," *IEE Proc. Gener. Transm. Distrib.,* vol. 143, no. 2, pp. 211–218, 1996.
[11] M. Noroozian and G. Anderson, "Damping of power system oscillations by use of controllable components," *IEEE Trans. PWRD*, vol. 9, no. 4, pp. 2046–2054, 1994.
[12] T. Hiyama, M. Mishiro, H. Kihara, and T. H. Ortmeyer, "Coordinated fuzzy logic control for series capacitor modules and PSS to enhance stability of power system," *IEEE Trans. PWRD*, vol. 10, no. 2, pp. 1098–1104, 1995.
[13] H. F. Wang and F. J. Swift, "A unified model for the analysis of FACTS devices in damping power system oscillations part I: single-machine infinite-bus power systems," *IEE Proc. Genet. Transm. Distrib.*, vol. 145, no. 2, pp. 111–116, 1998.
[14] Y. Y. Hsu and C. L. Chen, "Identification of optimum location for stabilizer applications using participation factors," *IEE Proc.*, pt. C, vol. 134, no. 3, pp. 238–244, May 1987.

[15] A. M. A. Hamdan, "An investigation of the significance of singular value decomposition in power system dynamics," *Int. Journal of Electrical Power and Energy Systems*, vol. 21, pp. 417–424, 1999.

[16] E. A Failat, M. Bettayyeb, H. Al-Duwaish, M. A. Abido, and A. Mantawy, "A neural network based approach for on-line dynamic stability assessment using synchronizing and damping torque coefficients," *Electrical Power Systems Research*, vol. 39, no. 2, pp. 103–110, 1996.

[17] F. Herrera, M. Lozano, and J. L. Verdegay, "Tackling real-coded genetic algorithms: operators and tools for behavioral analysis," Artificial Intelligence Review, vol. 12, no. 4, pp. 265–319, 1998.

Appendix

The system data are as follows:

$M = 9.26$ s	$T'_{do} = 7.76$	$D = 0.0$	$x_d = 0.973$
$x'_d = 0.19$	$x_q = 0.55$	$R = -0.034$	$X = 0.997$
$g = 0.249$	$b = 0.262$	$K_A = 50$	$T_A = 0.05$
$K_s = 1.0$	$T_s = 0.05$	$\|u_{PSS}\| \leq 0.2$ pu	$\|B_{SVC}\| = 0.4$ pu
$\|X_{TCSC}\| = 0.5X$	$\|\Phi_{TCSP}\| = 15^\circ$	$\|E_{fd}\| \leq 7.3$ pu	$v = 1.05$ pu.

All resistances and reactances are in pu, and time constants are in seconds.